Combinatorial Synthesis and Hydrogenation of Mg/Al Libraries Prepared by Electron Beam Physical Vapor Deposition

Gemma Garcia,[†] Roger Doménech-Ferrer,[†] Francesc Pi,[†] Josep Santiso,[‡] and Javier Rodríguez-Viejo*,[†]

Departament de Física, Universitat Autònoma de Barcelona, 08193 Bellaterra, Spain, and ICMAB/CSIC, Esfera UAB, Campus UAB, 08193 Bellaterra, Spain

Received September 19, 2006

We have grown thin film libraries of the Mg−Al system using a high-throughput synthesis methodology that combines the sequential deposition of pure elements (Mg and Al) by an electron-beam (e-beam) evaporation technique and the use of a special set of moving shadow masks. This novel mask has been designed to simultaneously prepare four identical arrays of different compositions that will permit the characterization of the same library after several treatments. Wavelength dispersive spectroscopy (WDS) and micro-X-ray diffraction have been used as high-throughput screening techniques for the determination of the composition and structure of every member of the library in the as-deposited state and after hydrogenation at 1 atm of H_2 during 24 h at three different temperatures: 60, 80, and 110 °C. We have analyzed the influence of the Mg−Al ratio on the hydrogenation of magnesium, as well as on the appearance of complex hydride phases. We have also found that aluminum can act as a catalyzer for the hydrogenation reaction of magnesium.

Introduction

The need for clean hydrogen energy systems demands the discovery of efficient solid-state hydrogen storage materials. An effective way to test different materials would be to join both a combinatorial synthesis method and a fast combinatorial screening technique. The present work is included in a larger study where a combinatorial electron-beam (e-beam) evaporation deposition technique and a multisystem nanocalorimetric device are developed and tested as combinatorial synthesis and screening techniques, respectively. For this purpose, we report in this paper the results in the preparation and characterization of binary libraries of metal hydrides based on the Mg−Al system.

Magnesium and magnesium-based alloys are one of the most attractive materials for hydrogen storage because of their high hydrogen-storage capacity (7.6 wt % for MgH_2), low density, and low cost. However, two major limitations should be overcome before the requirements for practical applications are fulfilled. (i) The high enthalpy of formation of MgH_2, around −76 kJ/molH_2, is responsible for the high-temperature release of hydrogen (552 K at 1 bar), and (ii) the slow hydriding and dehydriding kinetics make its application into real systems difficult. The alloying of Mg with heavy transition metals may result in compounds with lower formation enthalpy, as is the case of Mg_2NiH_4; however, this reduction comes at the expense of reducing storage capacity.[1] A possible and better solution would come from the addition of light metals with a lower affinity for hydrogen, such as Al or other light group elements. Moreover, according to Guo et al.,[2−3] the addition of Al to MgH_2 reduces the stability of the hydride leading to an improvement in the dehydrogenation conditions. The heat of formation predicted for the MgH_2 + Al system is 28 kJ/mol of H_2.[4] Moreover, it has also been reported that mixing magnesium with minor amounts of catalytic transition elements, such as Ti or Fe, effectively improves the hydriding and dehydriding kinetics of magnesium at high temperatures.[4] It is also now well-recognized that the nanocrystalline structure of new hydrides improves their hydrogen sorption/desorption kinetics.[5,6] The addition of light elements may also lead to the formation of complex hydrides, such as alanate compounds. In particular, $Mg(AlH_4)_2$ has a 9.3 wt % hydrogen storage capacity and, upon heating, releases hydrogen in two steps; the first one with an amount of 7 wt % results in the formation of MgH_2 and Al. Typically, Mg alanate is synthesized by lengthy chemical routes.[7−9] However, a recent theoretical work by van Setten et al.[10] predicts by computational methods that this phase is stable with respect to the pure elements and therefore may be synthesized by a direct route. In fact, some authors have already reported the formation of this compound from pure Mg−Al thin films under different conditions.[11−13]

Despite the fact that a large number of intermetallic alloys have been screened for hydrogen-storage potential, no one compound fits the accepted criteria for use in real applications. The search could be significantly accelerated using combinatorial and high-throughput methods. One of the easiest ways to couple a combinatorial synthesis with nanosized materials or alloys is to prepare thin film libraries using a physical vapor deposition (PVD) technique. This combinatorial approach has been successfully used in the

* To whom correspondence should be addressed. E-mail: javirod@vega.uab.es.
[†] Departament de Física, Universitat Autònoma de Barcelona.
[‡] ICMAB/CSIC, Esfera UAB.

10.1021/cc060131h CCC: $37.00
Published on Web 01/20/2007

search for phosphors, dielectric thin films, and advanced ceramics[14,15] and has also been introduced in the preparation of hydrogen-sorbing metal alloys.[12,13,16] Thin films show significant advantages over more extended ball-milling techniques since stoichiometry, structural order, and grain size can be better controlled and characterized. Furthermore, glassy metastable phases with unknown hydrogenation behavior may be encountered during growth or upon annealing treatments in H_2 atmosphere. In addition, in those systems, hydrogenation/dehydrogenation is not kinetically limited because of the short diffusion paths involved, and lower reaction temperatures can be used for an effective hydrogenation of the system.

This paper mainly focus on the analysis of the hydrogenation behavior in magnesium/aluminum hydride storage materials prepared as thin films using a combinatorial approach to synthesize many compositions simultaneously on a single substrate. A high-throughput screening technique such as X-ray microdiffraction is used to characterize in a reasonable amount of time a large number of compounds. The influence of the Mg−Al ratio on the hydrogenation of magnesium, as well as on the possible appearance of a complex hydride phase, is discussed.

Experimental Section

The films were prepared in a Leybold UNIVEX 450 e-beam evaporation setup at room temperature on glass substrates. The evaporation parameters were optimized individually to stabilize the growth rate of the different metals. The growth rates were determined, using a quartz microbalance located inside the deposition chamber, to be 0.2 nm/s at $P = 10^{-5}$ mbar, 0.15 nm/s at $P = 10^{-5}$ mbar, 0.2 nm/s at $P = 4 \times 10^{-6}$ mbar, and 0.25 nm/s at $P = 4 \times 10^{-6}$ mbar for Pd, Fe, Mg, and Al, respectively. The Mg/Al multilayers were sandwiched between Pd/Fe bilayers at both faces forming a multilayered system: Pd/Fe/(Mg + Al)/Fe/Pd. The palladium coating of 15 nm was deposited to ensure a fast dissociation rate and good transport properties for hydrogen, as well as to avoid oxidation of magnesium either from atmosphere or from the substrate surface. The Fe layer was deposited to prevent the formation of Mg_xPd_y intermetallics during the thermal treatments. The thickness of the Fe layer was formerly optimized and fixed at 10 nm to avoid interdiffusion for temperatures below 230 °C (Mg_6Pd was found for thinner films treated at temperatures above 200 °C), while keeping the hydrogenation possible.

To carry out the combinatorial vapor deposition, we used a special setup which is shown in Figure 1. We designed a set of U-shaped masks moving perpendicularly one to the other to obtain four identical libraries. In the starting mask position, the four square zones with identical area are exposed to the deposition of Pd and Fe. Then the masks are moved to a second position and sequential deposition of different Mg and Al film thickness starts. The Mg mask is translated from bottom to top of the library following seven discrete positions separated by 3 mm to grow seven rows with increasing thickness. The Mg mask is then removed from the active area, and the Al masks starts to move perpendicularly from the left to the right following an identical

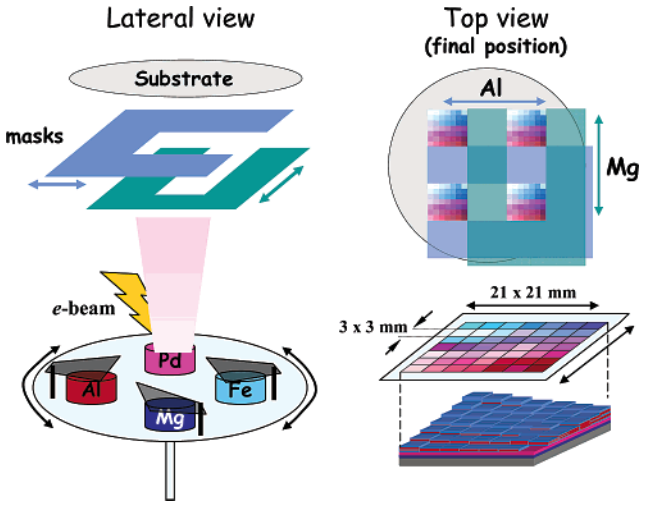

Figure 1. Scheme of the deposition setup. Four different elements can be evaporated. Mask system with a U shape is used to create four identical libraries 21 × 21 mm² size and with 49 (7 × 7) members of 3 × 3 mm² each.

Al (nm)

350	310	260	124	70	64	0	
175 Al x2	155 Al x2	130 Al x2	62 Al x2	35 Al x2	32 Al x2		0
25 Mg x3 175 Al x2	25 Mg x3 155 Al x2	25 Mg x3 130 Al x2	25 Mg x3 62 Al x2	25 Mg x3 35 Al x2	25 Mg x3 32 Al x2	25 Mg x3	75
42 Mg x3 175 Al x2	42 Mg x3 155 Al x2	42 Mg x3 130 Al x2	42 Mg x3 62 Al x2	42 Mg x3 35 Al x2	42 Mg x3 32 Al x2	42 Mg x3	126
50 Mg x3 175 Al x2	50 Mg x3 155 Al x2	50 Mg x3 130 Al x2	50 Mg x3 62 Al x2	50 Mg x3 35 Al x2	50 Mg x3 32 Al x2	50 Mg x3	150
58 Mg x3 175 Al x2	58 Mg x3 155 Al x2	58 Mg x3 130 Al x2	58 Mg x3 62 Al x2	58 Mg x3 35 Al x2	58 Mgx3 32 Al x2	58 Mg x3	175
67 Mg x3 175 Al x2	67 Mg x3 155 Al x2	67 Mg x3 130 Al x2	67 Mg x3 62 Al x2	67 Mg x3 35 Al x2	67 Mg x3 32 Al x2	67 Mg x3	201
83 Mg x3 175 Al x2	83 Mg x3 155 Al x2	83 Mg x3 130 Al x2	83 Mg x3 62 Al x2	83 Mg x3 35 Al x2	83 Mg x3 32 Al x2	83 Mg x3	249

Mg (nm)

Figure 2. Description of the Mg/Al library with the aluminum and magnesium layers thickness (in nm) of each member of the array.

seven position movement program. To achieve a direct intimate mixing of the Mg and Al elements and thus a better depth control of the net composition in each 3 × 3 mm² individual members, we deposited a multilayer Al−Mg system composed of two aluminum layers sandwiched by three magnesium layers that can be described as Mg/Al/Mg/Al/Mg. Varying the total thickness of Al from 0 to 350 nm (thicknesses of 0, 64, 70, 124, 260, 310, 350 nm) and Mg layers from 0 to 250 nm (thicknesses of 0, 75, 126, 150, 174, 201, 249 nm), controlling the deposition time, and moving the two masks as described above, we deposited an array of 49 members with selected Mg/Al compositions. The final Mg and Al thicknesses for each member are shown in Figure 2. Those values were selected to prepare Mg_xAl_{1-x} members with a large range of magnesium composition (x). The magnesium thickness is constant in each row and increases from top to bottom of the library, while the

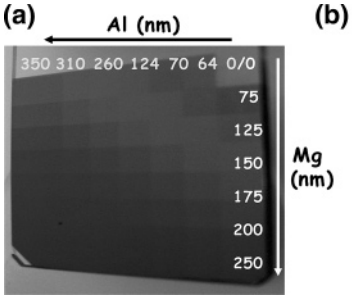

(b)

0	0	0	0	0	0	% at Mg
15	16	19	32	45	48	100
22	24	28	44	57	60	100
25	27	31	49	63	65	100
28	31	35	53	66	68	100
31	34	38	56	69	71	100
37	39	44	62	74	76	100

Figure 3. (a) Optical image of the as-deposited array. (b) Mg to Al composition (at. %) of the library determine by WDS.

aluminum thickness increases from the right to the left column. The deposition was programmed to obtain a first column/row of pure magnesium/aluminum of different thicknesses. The analysis of the pure Mg column is necessary to differentiate between the phenomena related to the presence of aluminum from the phenomena only related to the different thickness of magnesium.

The composition of the as-deposited library was determined by microanalysis using a CAMECA SX50 equipped with four wavelength-dispersive spectrometer detectors. Only Fe, Pd, Al, and Mg were detected. Special software (STRATAGEM) for thin films was used to determine the exact composition of the thin film members of the library without interference of the substrate composition.

The hydrogenation of the samples was done at 1 bar of hydrogen pressure during 24 h at three different temperatures (60, 80, and 110 °C) and on three different libraries. The structural characterization of the samples after hydrogenation, as well as the as-prepared samples, was performed by micro-X-ray diffraction in a Bruker D-8 Advance system coupled with a Gadds detector (Cu Kα, $\lambda = 1.5418$ Å). The system is equipped with a pinhole collimator of 0.5 mm diameter to perform microdifraction and a computer controlled XY stage to make programmed scans for each array position of the library. The acquisition time of a single frame spectra was fixed to 30 min to obtain enough signal intensity. Under the same conditions, we measured the glass substrate, and we used this blank pattern to subtract the background of the measured diffractograms.

Results and Discussion

As-Deposited Samples. Despite their metallic character, the 49 members of the as-deposited library could be visually differentiated, as shown in Figure 3a. The total composition of each member was determined by WDS resulting in a Mg/Al ratio very close to the values expected from their thickness. The atomic percentage of magnesium in every cell is indicated in Figure 3b

The as-deposited library was characterized by XRD. Only the reflections corresponding to the four metals were observed. For clarity, only members with a representative magnesium composition from 0 to 100% are plotted in Figure 4. The 110 reflection of bcc-Fe and the 111 reflection of fcc-Pd were observed in all the library members. As it can be seen in the X-ray patterns those two peaks were rather broad, as expected for thin layers of 15 and 10 nm for Pd and Fe, respectively. The 0002 reflection of the hcp-Mg

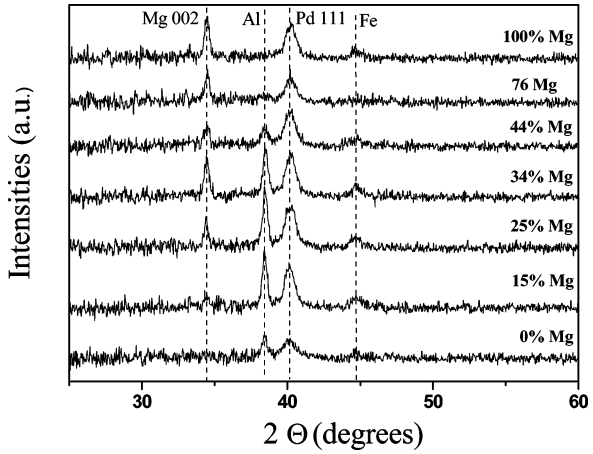

Figure 4. XRD patterns of selected cells of the as-deposited library. (The 0% corresponds to the thicker, 350 nm, Al members and the 100% corresponds to the thicker, 250 nm, Mg member of the library).

layer was the only one observed for all the members containing magnesium, confirming the preferred orientation along this direction for layers deposited by e-beam evaporation.[16] The 111 reflection of fcc-Al was also detected everywhere except on the right column without Al. It is interesting to note that the 0% Mg samples in Figure 4, which correspond to the thicker Al films (350 nm) of the library, show the lower peak intensities of the series, and they are especially lower than those of the 15 and 25% Mg samples that correspond to the same Al thickness, intercalated between Mg (175 Al $\times$ 2 + 25 Mg $\times$ 3 and 175 Al $\times$ 2 + 50 Mg $\times$ 3). This behavior is related to a stronger preferred orientation of the Al layer when it grows onto the columnar, highly oriented structure of Mg than onto the nanocrystalline Fe layer. No MgO was detected, confirming the utility of the Pd layers as barrier for oxidation. It is also worth mentioning that the preparation conditions of our layers, low-energetic growth of species along with deposition at room-temperature, did not give rise to the formation of Mg_xAl_{1-x} intermetallic or solid solutions in the as-prepared library, at least within the detection limits of the characterization technique. That fact gives us the opportunity not only to check the formation of new hydrides of the Mg_xAl_{1-x} system upon selected thermal treatments but also to check the influence of the presence of aluminum in the hydrogenation of pure magnesium members.

Hydrogenated Samples. The libraries were hydrogenated at 1 bar during 24 h at 60, 80, and 110 °C. By analysis of the right column composed only by Mg layers of different thickness by XRD, we were able to determine the influence of the thickness on the hydrogenation of the layers. For simplicity, we choose four representative magnesium thickness 75, 150, 200, and 250 nm, and we plotted the XRD patterns at various hydrogenation temperatures as can be seen in Figure 5.

When the hydrogenation temperatures are increased, the reflections corresponding to metallic Mg tend to disappear, and only the MgH_2 phase reflections are detected. Nevertheless, some differences appear in the comparison of thin and thick magnesium films. For cells hydrogenated at 60 °C (Figure 5.b), even for the thinner films, the magnesium layers

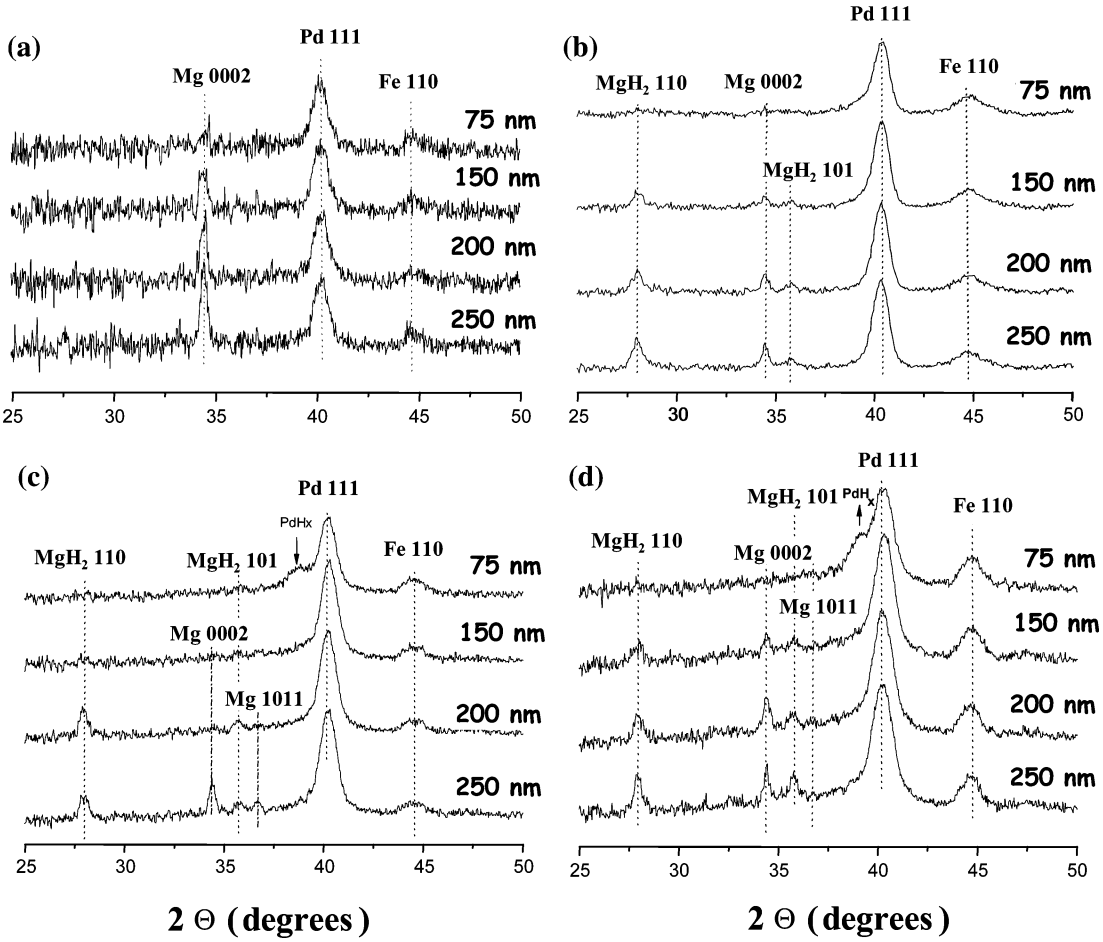

Figure 5. XRD pattern of hydrogenated pure magnesium cells: (a) as-deposited, (b) 60, (c) 80, and (d) 110 °C.

are not completely hydrogenated because we can detect, for any thickness, reflections corresponding to MgH_2 and Mg. For samples treated at 80 °C (Figure 5c), the detected phase changes as a function of thickness. The thinner films were completely hydrogenated, and no trace of pure magnesium was detected, although we have to note that the intensity signal of the MgH_2 peaks were still very weak. For thicker films, the 0002 and 1011 reflections of hcp-Mg, along with the diffraction lines associated to the MgH_2 phase, were identified. For samples hydrogenated at 110 °C (Figure 5c), the situation is quite similar; only the thinner samples were completely hydrogenated. It is very likely from such results that MgH_2 could act as a barrier for hydrogenation because of the limited diffusivity of hydrogen through the hydride phase. This behavior agrees with previous findings by numerous authors.[18] We have also to point out that for thinner Mg layers (75 nm) and for hydrogenation temperatures above 80 °C we detect the appearance of palladium hydride along with metallic palladium. Nevertheless, the peak intensity is weaker than the one associated to the Pd 111 line showing that the hydrogenation of the Pd layers after a treatment at 110 °C during 24 h was not complete. The formation of this hydride has already been observed on Pd capped Mg layers.[19] For thicker magnesium layers, regardless of the hydrogenation temperature, we did not observe the presence of PdH_x peaks in the XRD patterns. Therefore, the PdH_x reflection only appears for totally hydrogenated magnesium compounds, that is, the thinner Mg films members of the right column, and thus one can assess that the Pd layer partially transforms into a hydride phase if the magnesium has been totally hydrogenated before. We can conclude that even if the palladium capping layer seems to act efficiently as a catalyst for the hydrogenation reaction it is still rather difficult to hydrogenate thick magnesium films at these low temperatures. The threshold maximum thickness of total hydrogenation under such conditions seems to be around 75 nm. The presence of PdH_x could be used, at least with pure magnesium members, as a fingerprint of the total hydrogenation of the compounds.

There is another phenomenon that appears as a function of hydrogenation temperature for a constant Mg thickness. Films hydrogenated at 60 °C (Figure 5b) clearly showed the reflection corresponding to MgH_2 110 and 101 along with some Mg 0002 still remaining in the films. When the treatment temperature was increased to 80 °C, the reflections of MgH_2 become weaker, and along with the 0002, we start to observe also the 1011 reflection of magnesium. The hydrogenation at this temperature seems thus accompanied by a nanocrystallization process that gives rise to a lost of preferred orientation of the Mg crystallites. When the hydrogenation temperature was increased to 110 °C, the MgH_2 and the Mg peaks became more intense either because the hydrogenation increases, in the case of MgH_2, or because of the appearance of a recrystallization process, for both MgH_2 and Mg, resulting in an intensity increase.

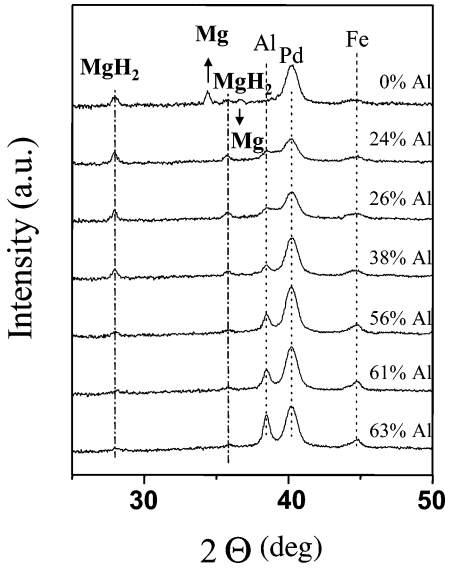

Figure 6. XRD spectra of samples with different Al compositions treated in 1 bar of hydrogen at 80 °C for 24 h.

The "aluminum-doped" members of the library have also been characterized after hydrogenation by XRD, and the results have been compared to pure magnesium films, giving rise to some interesting conclusions. As stated above there is a maximum Mg thickness that can be totally hydrogenated even at temperatures as low as 80 °C. To study the effect of aluminum layers introduced inside magnesium, we focus on the analysis of the hydrogenation of the bottom row of the library. This row corresponds to members with 250 nm of deposited magnesium but formed by three single-layers of 83 nm which is close to the maximum thickness (~75 nm) of pure Mg that we have been able to fully hydride. The different members of that row (from right to left) correspond to compounds with two single-layers of aluminum from 32 to 175 nm. In Figure 6, we plot the XRD patterns of that row after hydrogenation at 80 °C.

We can see that the reflections assigned to MgH_2 appear for all the Mg_xAl_{1-x} members of the row, while reflections corresponding to pure Mg completely vanish. We have thus been able to hydrogenate a magnesium amount equivalent to a 250 nm layer by intercalating aluminum layers. Apparently the aluminum layers do not act as barriers for hydrogenation but instead act as efficient path for an improved hydrogenation. We have to point out that the same phenomenon was observed for the samples treated at 110 °C. Despite the fact that the magnesium thickness is constant for all the XRD patterns of Figure 6, the (101) MgH_2 peak intensity decreases with increasing Al content. As will be discussed below, we believe this intensity attenuation is related to the formation of a complex hydride phase, different from MgH_2, at compositions close to 66 at. % Al.

The unexpected behavior of some specific members of the library hydrogenated at 80 °C can be distinguished in Figure 7 where we plot the XRD patterns of the 36 binary Mg_xAl_{1-x} members. We can identify a threshold value of around 33−35% at of Mg above which the intensity of the Al reflection decreases considerably.

A clear example of such phenomenon is shown in Figure 8 where the XRD patterns of the compound with 37 at. %

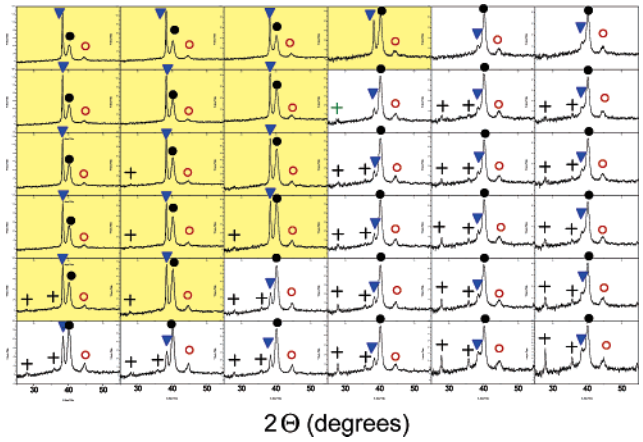

Figure 7. XRD patterns of the binary Mg_xAl_{1-x} members of the library. Frames in yellow correspond to members with $x < 35$ at. % Mg (▼ = Al, ● = Pd, ○ = Fe, + = MgH_2). The intensity scale for all the library frames is the same.

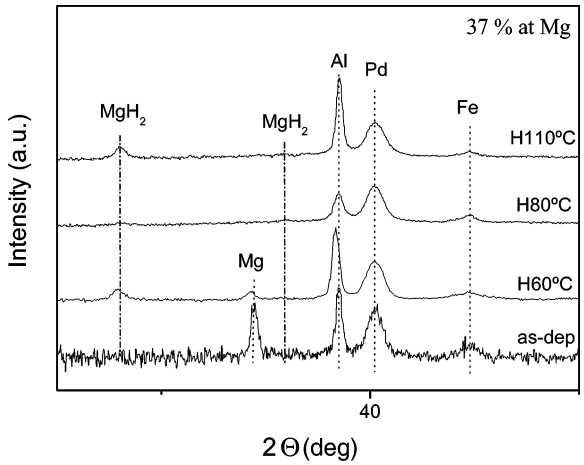

Figure 8. Micro-XRD patterns of a member of the library with a total amount of 37 at. % of Mg in the as-prepared state and hydrogenated at temperatures of 60, 80, and 110 °C.

of magnesium hydrogenated at different temperatures are plotted for comparison. Hydrogenation temperatures above or equal to 80 °C resulted in a total hydrogenation of the sample.

Figure 8 shows that along with the weak intensity of the MgH_2 reflections at 80 °C there is a reduction of the Al 111 peak area. This decrease has only been detected for samples with compositions above 33−35 at. % Mg. To analyze this behavior in more detail, we plot, in Figure 9, the ratio of the area of the aluminum 111 reflection of the samples treated at 60 °C upon the area of the same cells treated at 80 °C, A_{111}(60 °C)/A_{111}(80 °C). This ratio does not depend on the thickness of the layers. We can identify the presence of two different regions. At $x \leq 33-35$ at. % Mg the ratio is close to 1, while at higher Mg concentrations, the ratio is above 1. This behavior cannot be associated to the formation of AlH_3 since this hydride has such a high pressure in equilibrium with the gas phase that in practice cannot be formed from the gas. Moreover, the analysis of the pure Al members of the library did not reveal any significant change of the overall Al 111 intensity upon hydrogenation. The above statements suggest that the Al decrease at 80 °C could be caused by the formation of either some amorphous

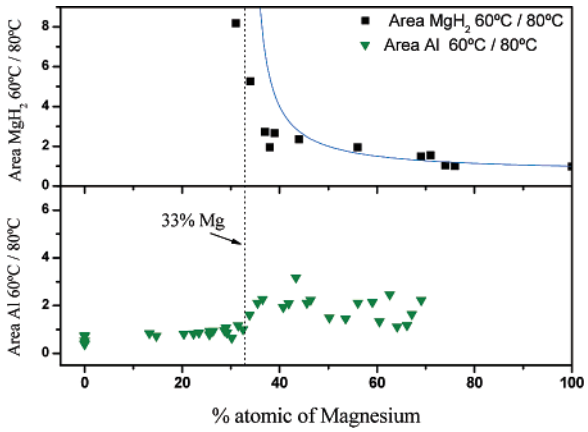

Figure 9. Area of MgH_2 (upper image) and (111) Al at 60 °C divided by the corresponding areas at 80 °C as a function of Mg content. The continuous line in the upper figure represents the theoretical ratio of MgH_2 considering that $Mg(AlH_4)_2$ has been formed at 80 °C.

intermetallic alloy or another hydride phase. It is tempting to relate this behavior to the presence in our samples of Mg alanate ($Mg(AlH_4)_2$), because we observed it for compositions higher than 33−35 at. %, which is close to the expected Mg/Al atomic ratio in this complex hydride. The fact that no X-ray signal from this crystalline phase was identified in the X-ray diffraction spectra could be either the result of its low scattering factor or of the fact that only a small percentage of the Mg and Al atoms, those present in the intermixed regions at the interfaces, participate in this compound. Gremaud et al.[12,13] have recently detected in Al/Mg thin films, around this composition, a strange behavior in the optical transmission of the films. They have assigned these anomalies to the formation of the alanate. However, given the experimental evidence, we cannot completely rule out the possible formation of an amorphous intermetallic alloy. At 110 °C and for $x > 35-40$ at. % Mg, the overall Al intensity increases again (not shown). In our opinion, this may be explained by a segregation phenomena resulting from the dissociation of $Mg(AlH_4)_2$ into MgH_2 and Al.

Another point which further supports the presence of an unidentified hydride phase is the behavior of the MgH_2 X-ray diffraction peaks. The (110) MgH_2 peak is usually small, and therefore, its analysis may be subject to larger uncertainties. Despite this, a general trend can also be schematically drawn comparing the area of the MgH_2 (110) peak at 60 °C divided by the total area of MgH_2 (110 and 101 peaks) at 80 °C of the two lower rows of the library (see Figure 9). These two rows are those with the highest Mg thickness and therefore where the Mg and related hydride peaks are better identified. At compositions ranging from 30 to 40 at. % Mg, we again observe an anomalous behavior. The ratio of the areas increases to values of around 3−8, whereas for higher magnesium compositions, the ratio decreases again toward the value for pure Mg. If the only hydride phase was magnesium hydride one should not expect such a distinct behavior. Instead, in the composition range close to 33 at. % Mg, the formation of $Mg(AlH_4)_2$ is favored, and only those Mg atoms located far away from the interface with the Al atoms may contribute to the MgH_2 growth at this temperature. In the graph, the continuous line represents the theoretical dependence of the area ratio assuming that at 80 °C all the present aluminum has contributed to the formation of the alanate and the remaining magnesium has been hydrogenated into MgH_2. We can see a clear correspondence between the experimental data and the simplified assumption. Nevertheless, complementary analysis should be performed to assess the formation of the $Mg(AlH_4)_2$ phase from the pure elements.

Conclusions

We report the sequential deposition of Mg/Al layers covered with Fe/Pd using combined e-beam evaporation with moving masks to produce discrete libraries with a wide composition range. High-throughput screening of the structure of the libraries in the as-deposited state and after hydrogenation is achieved by X-ray microdiffraction. For all the Mg/Al compositions, a complete hydrogenation of the samples was possible at much lower temperatures compared to bulk samples. We have demonstrated that the addition of aluminum improves the hydrogenation of magnesium. MgH_2 was the main crystalline hydride phase observed for all the compositions, above 20 at. % Mg. For lower contents, the thickness of the Mg layers was too small to detect any crystalline phase associated either to pure hcp-Mg or to the hydride. For members with composition above 33−35 at. % Mg, a change in the hydrogenation behavior detected by changes in the X-ray patterns suggest the possible presence of a complex hydride phase, probably $Mg(AlH_4)_2$. This phase may only represent a small fraction of the whole layer; direct X-ray evidence of its formation is still unachieved, and further work is underway.

Acknowledgment. The authors acknowledge financial support from Air Products and Chemicals, MATGAS 2000 AIE, the Spanish Ministry of Education under Project MAT2004-04761, and the Direcció General de Recerca of the Generalitat de Catalunya under Project 2005SGR00201.

References and Notes

(1) Goo, N. H.; Woo, J. H.; Lee K. S. *J. Alloys Compd*. **1999**, *288*, 286−291.
(2) Bououdina, M.; Guo, Z. X. *J. Alloys Compd.* **2002**, *336*, 222−231.
(3) Song, Y.; Guo, Z. X.; Yang, R. *Phys. Rev. B* **2004**, *69*, 094205.
(4) Shang, C. X.; Bouodina, M.; Song, Y.; Guo, Z. X. *Int. J. Hydrogen Energy* **2004**, *29*, 73−80.
(5) Zaluska, A.; Zaluski, L.; Ström-Olsen, J. O. *J. Alloys Compd.* **1999**, *288*, 217−225.
(6) Zaluska, A.; Zaluski, L.; Ström-Olsen, J. O. *Appl. Phys. A* **2001**, *72*, 157−165.
(7) (a) Fichtner, M.; Engel, J.; Fuhr, O.; Gloss, A.; Rubner, O.; Ahlrichs, R. *Inorg. Chem.* **2003**, *42*, 7060−7066. (b) Fichtner, M.; Fuhr, O.; Kircher, O.; *J. Alloys Compd.* **2003**, *356−357*, 418−422.
(8) Mamatha, M.; Bogdanovic, B.; Felderhoff, M.; Pommerin, A.; Schmidt, W.; Schuth, F.; Weidenthaler, C. *J. Alloys Compd.* **2006**, *407*, 78−86.
(9) Varin, R. A.; Chiu, Ch.; Czujko, T.; Wronski, Z. *Nanotechnology* **2005**, *16*, 2261−2274.

(10) van Setten, M. J.; de Wijs, G. A.; Popa, V. A.; Brocks, G. *Phys. Rev. B* **2005**, *72*, 073107.
(11) Pranevicius, L. L.; Milcius, D. *Thin Solid Films* **2005**, *483*, 135−140.
(12) Gremaud, R.; Borgschulte, A.; Chacon, C.; Van Mechelen, J. L. M.; Schereuders, H.; Züttel, A.; Hjörvarsson, B.; Dam, B.; Griessen, R. *Appl. Phys. A* **2006**, *84*, 77−85.
(13) Gremaud, R.; Borgschulte, A.; Schereuders, H.; Züttel, A.; Dam, B.; Griessen, R. *J. Alloys Compd.* **2005**, *404*−*406*, 775−778.
(14) Hanak, J. J. *J. Mater. Sci.* **1970**, *5*, 964−971.
(15) Zhao, J. C. *Prog. Mater. Sci.* **2006**, *51*, 557−631.
(16) Olk, C. H.; Tibbetts, G. G.; Simon, D.; Moleski, J. J. *J. Appl. Phys.* **2003**, 94 p.720−725.
(17) Rodríguez-Viejo, J.; Gonzalez-Silveira, M.; Clavaguera-Mora, M. T. *J. Appl. Phys.*, **2003**, *93*, 4447−4453.
(18) Vegge T. *Phys. Rev. B* **2004**, *70*, 035412 and references therein.
(19) Higuchi, K.; Yamamoto, K.; Kajioka, H.; Toiyama, K.; Honda, M.; Orimo, S.; Fujii, H. *J. Alloys Compd.* **2002**, *330*−*332*, 526−530.

CC060131H